Annals of Nuclear Medicine (2019) 33:733–739
https://doi.org/10.1007/s12149-019-01383-4

ORIGINAL ARTICLE

Al^{18}F-labeled alpha-melanocyte-stimulating hormone (α-MSH) peptide derivative for the early detection of melanoma

Citra R. A. P. Palangka[1] · Hirofumi Hanaoka[2] · Aiko Yamaguchi[2,3] · Takashi Murakami[4] · Yoshito Tsushima[1,5]

Received: 9 May 2019 / Accepted: 28 June 2019 / Published online: 5 July 2019

Abstract

Objective Early detection plays a role in the prognosis of melanoma, the most aggressive skin cancer. ^{64}Cu- and ^{68}Ga-labeled alpha-melanocyte-stimulating hormone (α-MSH) analogs targeting the melanocortin-1 receptor are promising positron emission tomography (PET) tracers for detecting melanoma, and the use of ^{18}F-labeling will further contribute to the detectability and availability. However, the high radiochemistry demand related to the conventional ^{18}F-labeling methods has restricted the development of ^{18}F-labeled α-MSH analogs. A recently developed radiofluorination method using aluminum-fluoride (Al^{18}F) offers a simple, efficient, and time-saving labeling procedure compared to the conventional ^{18}F-labeling methods. Herein, we sought to establish a simple preparation method for an ^{18}F-labeled α-MSH analog using Al^{18}F, and we examined its potential for the early detection of melanoma.

Methods A 1,4,7-triazacyclononane-*N*,*N*′,*N*″-triacetic acid (NOTA)-conjugated α-MSH analog (NOTA-GGNle-CycMSH$_{hex}$) was prepared by the Fmoc solid-phase strategy. NOTA-GGNle-CycMSH$_{hex}$ was labeled with Al^{18}F by heating at 105 °C using a microwave synthesizer for 15 min. Biodistribution study was conducted on B16/F10-luc melanoma-bearing mice at 30 min, 1 h and 3 h after injection of Al^{18}F-NOTA-GGNle-CycMSH$_{hex}$. PET imaging was conducted on melanoma-bearing mice at 1 h post-injection. One day prior to the PET imaging, bioluminescence imaging was also performed.

Results Al^{18}F-NOTA-GGNle-CycMSH$_{hex}$ was readily prepared with a high radiochemical yield (94.0 ± 2.8%). The biodistribution study showed a high accumulation of Al^{18}F-NOTA-GGNle-CycMSH$_{hex}$ in the tumor at 30 min and 1 h post-injection (6.69 ± 1.49 and 7.70 ± 1.71%ID/g, respectively). The tumor-to-blood ratio increased with time: 3.46 ± 0.89, 12.67 ± 1.29, and 35.27 ± 9.12 at 30 min, 1 h, and 3 h post-injection, respectively. In the PET imaging, Al^{18}F-NOTA-GGNle-CycMSH$_{hex}$ clearly visualized the tumors and depicted very small tumors (< 3 mm).

Conclusions We successfully prepared Al^{18}F-NOTA-GGNle-CycMSH$_{hex}$ in a simple and efficient manner. Al^{18}F-NOTA-GGNle-CycMSH$_{hex}$ showed high tumor accumulation and clearly visualized very small tumors in melanoma-bearing mice. These findings suggest that Al^{18}F-NOTA-GGNle-CycMSH$_{hex}$ will be a promising PET tracer for melanoma imaging at an earlier stage.

Keywords Melanoma · PET · Alpha-melanocyte-stimulating hormone · Fluoride–aluminum chelate · Peptide

✉ Hirofumi Hanaoka
hanaokah@gunma-u.ac.jp

[1] Department of Diagnostic Radiology and Nuclear Medicine, Gunma University Graduate School of Medicine, 3-39-22 Showa, Maebashi 371-8511, Japan

[2] Department of Bioimaging Information Analysis, Gunma University Graduate School of Medicine, 3-39-22 Showa, Maebashi 371-8511, Japan

[3] Texas Therapeutics Institute, The Brown Foundation Institute of Molecular Medicine, The University of Texas Health Science Center at Houston, Houston, TX 77054, USA

[4] Faculty of Medicine, Saitama Medical University, 38 Moro-Hongo, Moroyama 350-0495, Japan

[5] Research Program for Diagnostic and Molecular Imaging, Division of Integrated Oncology Research, Gunma University Initiative for Advanced Research (GIAR), Gunma University Graduate School of Medicine, 3-39-22 Showa, Maebashi 371-8511, Japan

Introduction

Melanoma is the most aggressive type of skin cancer, and its incidence is increasing [1]. Distant metastatic melanoma is associated with a poor prognosis. However, the overall 5-year survival rate can reach 98% if the melanoma is detected at its earliest stages and removed surgically [2]. Early detection and accurate staging thus play important roles in the management of melanoma.

Positron emission tomography (PET), a powerful tool for diagnostic imaging, is used for the detection and full staging of metastatic melanoma [3–5]. Although 2-^{18}F-fluoro-2-deoxy-glucose (^{18}F-FDG)-PET is the best examination for localized stage III/IV melanoma, there are several limitations to the use of ^{18}F-FDG-PET, including its low sensitivity to detect primary and metastatic lesions among stage I/II melanomas, the lack of small lesion detectability (< 5 mm) [6–8], and low specificity in distinguishing a malignant tumor from an inflammatory lesion [9]. Moreover, a certain subtype of melanoma that uses non-glucose-based substrates as an energy source does not take in much ^{18}F-FDG [10]. The development of PET tracers targeting melanoma-specific molecules could contribute to the early detection of melanoma.

Various radiolabeled alpha-melanocyte-stimulating hormone (α-MSH) peptide derivatives have been developed as melanoma-specific imaging probes [11–13]. These peptides specifically bind to melanocortin-1 (MC1) receptor, which is over-expressed on the surface of human melanoma cells [14]. Among the α-MSH derivatives, ^{64}Cu- or ^{68}Ga-labeled NOTA-GGNle-CycMSH$_{hex}$ (that is, 1,4,7-triazacyclononane-1,4,7-triacetic acid-conjugated Gly–Gly-Nle-c[Asp-His-D-Phe-Arg-Trp-Lys]-CONH$_2$, Fig. 1) has shown promising properties such as high tumor uptake and high tumor specificity in melanoma-bearing mice [15, 16]. However, limitations related to the use of ^{64}Cu and ^{68}Ga have restricted the wide use of these tracers [17–19]. Although the use of ^{18}F mitigates radioisotope-associated concerns, there are a limited number of ^{18}F-labeled α-MSH derivatives [20] because the high radiochemistry demand for the traditional ^{18}F-labeling methods has hindered the development of such derivatives [21, 22].

The recently discovered radiofluorination method using aluminum–fluoride (Al^{18}F) offers a simple, efficient, and time-saving labeling procedure compared to the conventional ^{18}F-labeling methods [23]. Similar to ^{64}Cu and ^{68}Ga, Al^{18}F coordinates a stable complex with NOTA [23, 24]. Some Al^{18}F-labeled peptides have already shown promising results in clinical studies [25, 26]. We hypothesized that the application of Al^{18}F-labeling to NOTA-GGNle-CycMSH$_{hex}$ could lead to the development of highly convenient ^{18}F-labeled α-MSH derivatives without compromising the promising properties of the original ^{64}Cu- and ^{68}Ga-labeled tracers while minimizing the complications related to the tracer availability.

In this study, we established a facile ^{18}F-labeling method for the preparation of Al^{18}F-NOTA-GGNle-CycMSH$_{hex}$. We evaluated the biodistribution profiles of Al^{18}F-NOTA-GGNle-CycMSH$_{hex}$ and the image quality and detectability of Al^{18}F-NOTA-GGNle-CycMSH$_{hex}$-PET in melanoma-bearing mice.

Materials and methods

Amino acids and reagents for peptide synthesis were purchased from Watanabe Chemical Industries (Hiroshima, Japan) and Merck (Darmstadt, Germany). The 1,4,7-triazacyclononane-1,4-*bis*-*tert*-butyl acetate-7-acetic acid [NOTA-*bis*(*t*Bu ester)] was purchased from Macrocyclics (Dallas,

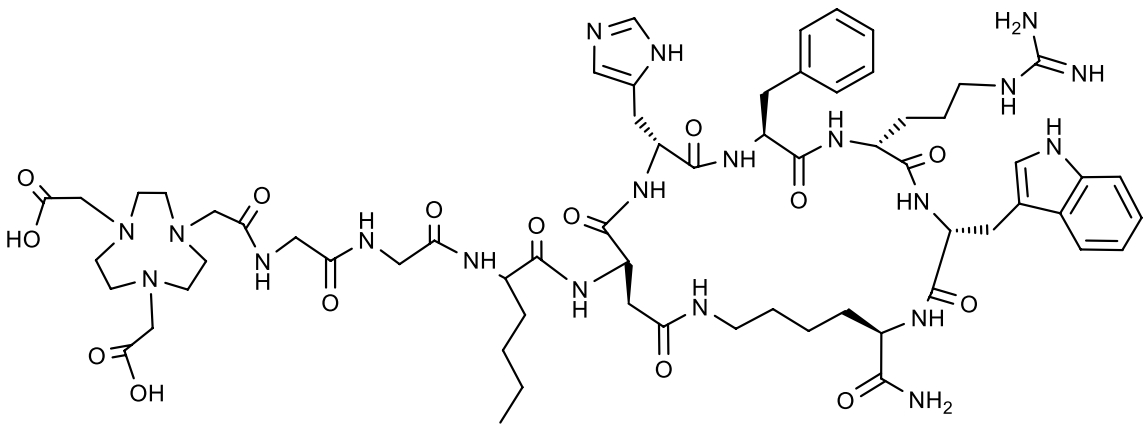

Fig. 1 The structure of NOTA-GGNle-CycMSH$_{hex}$

TX). Electrospray ionization mass spectroscopy (ESI–MS) data were obtained with a model LCMS-2020 mass spectrometer (Shimadzu, Kyoto, Japan).

Synthesis of precursor peptide

NOTA-GGNle-CycMSH$_{hex}$ peptide was synthesized as described by Shamshirian et al. [27] with slight modification. The linear peptide (Gly–Gly-Nle-Asp(O-2-PhiPr)-His(Trt)-D-Phe-Arg(Pbf)-Trp(Boc)-Lys(Mtt)-CONH$_2$) was synthesized using Fmoc solid-phase synthesis on Sieber amide resin with a fully automated peptide synthesizer (Initiator+ Alstra, Biotage Japan, Tokyo). Then, NOTA-*bis*(*t*Bu ester) was conjugated to the *N*-terminus of the linear peptide. The NOTA conjugate peptide was cleaved, and Asp(O-2-PhiPr) and the Lys(Mtt) were selectively deprotected in a single treatment of 2.5% trifluoroacetic acid (TFA) in dichloromethane for 15 min. The product was purified by RP-HPLC (column: CAPCELL PACK C18, AQ, 20 mm × 250 mm, Shiseido, Tokyo) with acetonitrile/0.1% TFA (A) and water/0.1% TFA (B) at a flow rate of 15 mL/min, and a linear gradient from 90 to 10% B in 30 min. The fraction containing the NOTA-conjugated linear peptide was collected, and the solvent was removed by freeze-drying. ESI–MS Calc'd for $C_{109}H_{150}N_{20}O_{21}S$ $(M+2H)^{2+}$: *m*/*z* 1053.4, found: 1054.2.

The NOTA-conjugated linear peptide (15 mg; 7.1 µmol) was dissolved in 15 mL of *N*,*N*-dimethylformamide and cyclized using benzole-1-yl-oxytris-pyrrolidino-phosphonium-hexafluorophosphate (PyBOP) (29.5 mg, 56.8 µmol) and *N*,*N*-diisopropylethylamine (19.3 µL, 113.6 µmol). The product was purified by RP-HPLC. ESI–MS Calc'd for $C_{109}H_{148}N_{20}O_{20}S$ $(M+2H)^{2+}$: *m*/*z* 1044.5, found: 1045.2.

The NOTA-conjugated cyclized peptide was deprotected using a mixture of anisole, 1,2-ethanedithiol, thioanisole, and TFA (2.5:2.5:5:90 v/v). The final product NOTA-GGNle-CycMSH$_{hex}$ peptide was purified by RP-HPLC. ESI–MS Calc'd for $C_{64}H_{93}N_{20}O_{15}$ $(M+H)^{+}$: *m*/*z* 1381.7, found: 1381.9.

Nonradioactive fluorine was used for preparing cold AlF-NOTA-GGNle-CycMSH$_{hex}$. First, NOTA-GGNle-CycMSH$_{hex}$ (450 µL, 2 mM) in acetate buffer (pH 4.0) was added to a mixture of aluminum chloride (360 µL, 5 mM) in 0.2 M acetate buffer (pH 4.0) and sodium fluoride (36 µL, 100 mM). The mixture was heated at 105 °C using a microwave synthesizer (Initiator+, Biotage) for 15 min. The product was purified by RP-HPLC (column: CAPCELL PACK C18, AQ, 4.6 mm × 250 mm, Shiseido) with acetonitrile/0.1% TFA (A) and water/0.1% TFA (B) at a flow rate of 1 mL/min, and a linear gradient from 85 to 65% B in 30 min. The fraction containing the peptide was collected, and the solvent was removed by freeze-drying. ESI–MS Calc'd for $C_{64}H_{91}AlFN_{20}O_{15}$ $(M+H)^{+}$: *m*/*z* 1425.7, found: 1425.9.

Radiolabeling with Al^{18}F

NOTA-GGNle-CycMSH$_{hex}$ (30 µL, 1 mM) in 1 M acetate buffer (pH 4.0) was added to a mixture of aluminum chloride (3 µL, 5 mM) in 0.2 M acetate buffer (pH 4.0), 0.1 mL of aqueous ^{18}F-fluoride (100 µL, 60–100 MBq), and ethanol (130 µL). The mixture was heated at 105 °C using a microwave synthesizer for 15 min. Al^{18}F-NOTA-GGNle-CycMSH$_{hex}$ was purified by RP-HPLC according to the retention time of nonradioactive AlF-NOTA-GGNle-CycMSH$_{hex}$ using the same gradient.

In vitro stability

First, 15 µL of Al^{18}F-NOTA-GGNle-CycMSH$_{hex}$ peptide in saline (1.5 MBq) was added to 135 µL of mouse serum, and the mixture was incubated for 0 h, 3 h, or 6 h at 37 °C. The sample was deproteinized using acetonitrile and analyzed by RP-HPLC (column: CAPCELL PACK C18, AQ, 4.6 mm × 250 mm) with acetonitrile/0.1% TFA (A) and water/0.1% TFA (B) at a flow rate of 1 mL/min, and a linear gradient from 90 to 10% B in 30 min.

Biodistribution study in C57BL/6 mice bearing a B16/F10-luc tumor

All animal experiments were approved by the animal experiments committee of Gunma University. The luciferase stably expressing the mouse melanoma cell line B16/F10-luc was purchased from Japanese Collection of Research Bioresources Cell Bank (Tokyo). The B16/F10-luc cells (2.5×10^5 cells/mouse) were subcutaneously injected on the right flank of C57BL/6 female mice (Japan SLC, Shizuoka, Japan). The tumor volume (*V*) was measured using digital calipers with the formula $V\,[mm^3] = (L \times W^2)/2$, where *L* represents the longest diameter and *W* represents the perpendicular tumor diameter. After the tumor size reached 100 mm^3 (approx. 2 weeks after cell inoculation), a biodistribution study was performed. Al^{18}F-NOTA-GGNle-CycMSH$_{hex}$ (200 kBq/mouse) was intravenously injected into B16/F10-luc tumor-bearing mice. Mice were killed at 30 min, 1 h, and 3 h after injection ($n \geq 4$, each group). The tissues of interest were harvested and weighed, and the radioactivity was counted using a gamma counter (ARC7001; Hitachi Aloka Medical, Tokyo). The results are presented as the percentage of injected dose per gram of tissue (%ID/g).

Bioluminescence and PET imaging

The B16/F10-luc cells were suspended in a mixture of PBS:Matrigel (Corning Life Sciences, Corning, NY) (1:1; v/v) at several cell densities (2×10^6, 1×10^6, 5×10^5, and

2.5×10^5 cells per 100 µL). Five-week-old female nude mice (BALB/c nu/nu, Japan SLC) were divided into two groups. Each mouse was injected subcutaneously with 100 µL of the cell suspension into the dorsal flank at two sites: the left and right. The mice in group 1 were injected with 2×10^6 and 1×10^6 cells/mouse, and the other group's mice were injected with 5×10^5 and 2.5×10^5 cells/mouse ($n = 3$, each group).

Small-animal PET imaging was performed when the tumor lengths were < 5 mm (approx. 1 week post-inoculation). B16/F10-luc tumor-bearing mice were intravenously injected with approx. 3 MBq/mouse of $Al^{18}F$-NOTA-GGNle-CycMSH$_{hex}$. PET imaging in list mode was carried out on an animal PET scanner (Inveon; Siemens, Knoxville, TN) at 1 h post-injection and with a 10 min acquisition time. The imaging data were reconstructed using an iterative OSEM3D/MAP procedure with the matrix size $128 \times 128 \times 159$, including attenuation correction. Immediately after the imaging, the tumor was removed and its volume was measured with calipers.

The bioluminescence imaging (BLI) was performed 1 day prior to the PET imaging. D-luciferin solution (15 mg/mL, 150 µg/g of body weight) was intraperitoneally injected to B16/F10-luc tumor-bearing mice under isoflurane-inhalation anesthesia. At 15 min after the injection, bioluminescence images were acquired with an IVIS Imaging System (PerkinElmer, Waltham, MA).

Results

Radiolabeling

$Al^{18}F$-NOTA-GGNle-CycMSH$_{hex}$ was successfully obtained within 60 min at a high radiochemical yield: 94.0 ± 2.8% ($n = 3$). Complete separation from its precursor peptide was achieved by RP-HPLC purification (Fig. 2). The retention times of $Al^{18}F$-NOTA-GGNle-CycMSH$_{hex}$ and its precursor peptide were 23.8 min and 21.5 min, respectively. After purification, the radiochemical purity of $Al^{18}F$-NOTA-GGNle-CycMSH$_{hex}$ was > 98%. The specific activity was 20–70 GBq/µmol at the end of synthesis.

In vitro stability

The in vitro stability of the radiotracer in murine serum was evaluated with the use of RP-HPLC. After incubation in murine serum at 37 °C for 6 h, the purity of the radiotracer remained high, and > 95% of the $Al^{18}F$-NOTA-GGNle-CycMSH$_{hex}$ remained intact (Fig. 3).

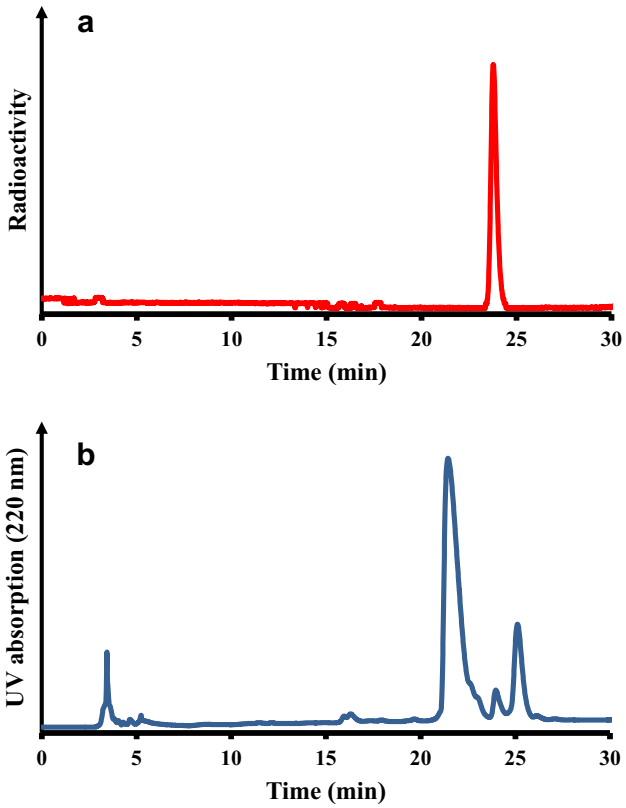

Fig. 2 An RP-HPLC chromatogram of $Al^{18}F$-NOTA-GGNle-CycMSH$_{hex}$ before purification. **a** UV and **b** radioactivity. The retention times of $Al^{18}F$-NOTA-GGNle-CycMSH$_{hex}$ and its precursor peptide (NOTA-GGNle-CycMSH$_{hex}$) were 23.8 min and 21.5 min, respectively

Biodistribution study

The biodistribution of $Al^{18}F$-NOTA-GGNle-CycMSH$_{hex}$ in B16/F10-luc tumor-bearing mice is summarized in Fig. 4. $Al^{18}F$-NOTA-GGNle-CycMSH$_{hex}$ showed high accumulation in the tumors at 30 min and at 1 h post-injection (6.69 ± 1.49 and 7.70 ± 1.71%ID/g, respectively), then decreased at 3 h post-injection (3.74 ± 0.77%ID/g). Due to the rapid blood clearance of $Al^{18}F$-NOTA-GGNle-CycMSH$_{hex}$, the tumor-to-blood ratio increased with time: 3.46 ± 0.89, 12.67 ± 1.29, and 35.27 ± 9.12 at 30 min, 1 h, and 3 h post-injection, respectively. The mouse kidneys, which are the excretory organ for MSH peptide [15, 16], showed the highest uptake at 30 min (8.46 ± 3.09%ID/g). The radioactivity accumulation gradually decreased with time (5.52 ± 0.57%ID/g and 2.39 ± 0.96%ID/g at 1 h and 3 h post-injection, respectively), which resulted in a tumor-to-kidney ratio that was > 1.0 after 1 h post-injection. The radioactivity uptake in the other normal tissues was < 2.4%.

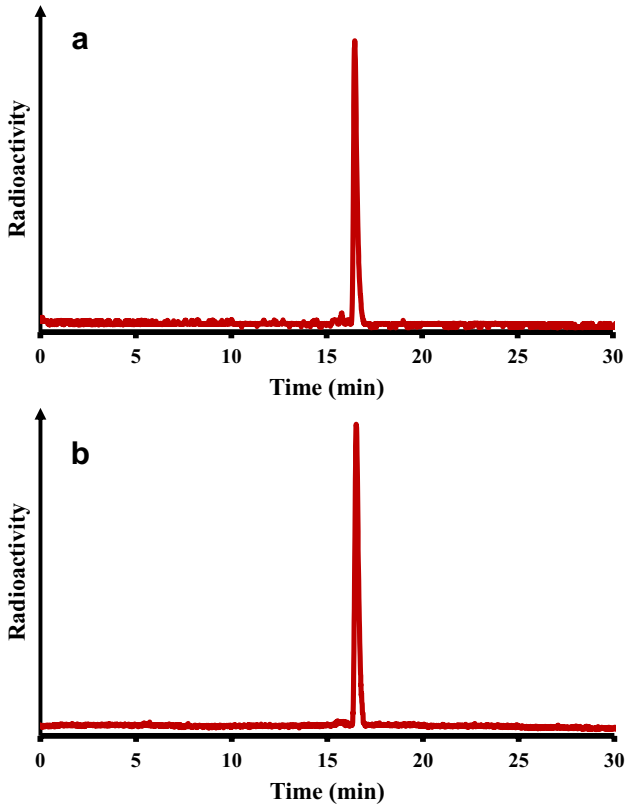

Fig. 3 A radio-chromatogram of $Al^{18}F$-GGNle-$CycMSH_{hex}$ after **a** 0-h and **b** 6-h incubation in mouse serum. The retention time of $Al^{18}F$-GGNle-$CycMSH_{hex}$ is 16.5 min

Bioluminescence and PET imaging

To evaluate the detectability of $Al^{18}F$-NOTA-GGNle-$CycMSH_{hex}$, we performed PET imaging when the murine tumors were small. At 1 week after the inoculation of B16/F10-luc cells at the densities of 2×10^6, 1×10^6, 5×10^5, and 2.5×10^5 cells per 100 µL, small tumors (4.5 ± 1.8 to 15.4 ± 3.5 mm^3) had developed. The location and formation of these small tumors were confirmed by bioluminescence imaging. In the PET images, high radioactivity uptake was observed in areas corresponding to bioluminescence signals (Fig. 5). $Al^{18}F$-NOTA-GGNle-$CycMSH_{hex}$ clearly depicted tumors as small as 3 mm (9 mm^3). A high accumulation of $Al^{18}F$-NOTA-GGNle-$CycMSH_{hex}$ was also noted in excretory organs for the radiotracer (kidney and bladder).

Discussion

Fluorine-18 is the most frequently used positron emitter in clinical practice. Almost all cyclotron facilities can produce ^{18}F anion with high activity and at moderate production costs. The lactam-bridged α-MSH analog NOTA-GGNle-$CycMSH_{hex}$ labeled with either ^{68}Ga or ^{64}Cu has been attracting attention due to the excellent pharmacokinetics and in vivo stability. While promising, the low availability and high cost of the radioisotopes have restricted the application of these tracers. In the present study, we developed a highly efficient ^{18}F-labeling method for NOTA-GGNle-$CycMSH_{hex}$ without any structural modification to the original peptide or complicated radiochemistry demands.

In contrast to the traditional nucleophilic ^{18}F-fluorination methods [28], $Al^{18}F$-NOTA-GGNle-$CycMSH_{hex}$ was readily prepared with an almost quantitative radiochemical yield ($94.0\pm2.8\%$), which is comparable to the radiochemical yields achievable with radiometal labeling [29]. Once the optimal radiolabeling protocol is established, it will be able to constantly produce $Al^{18}F$-NOTA-GGNle-$CycMSH_{hex}$ with radiochemical yields higher than 95%. This will allow for the omission of the purification process, a drawback

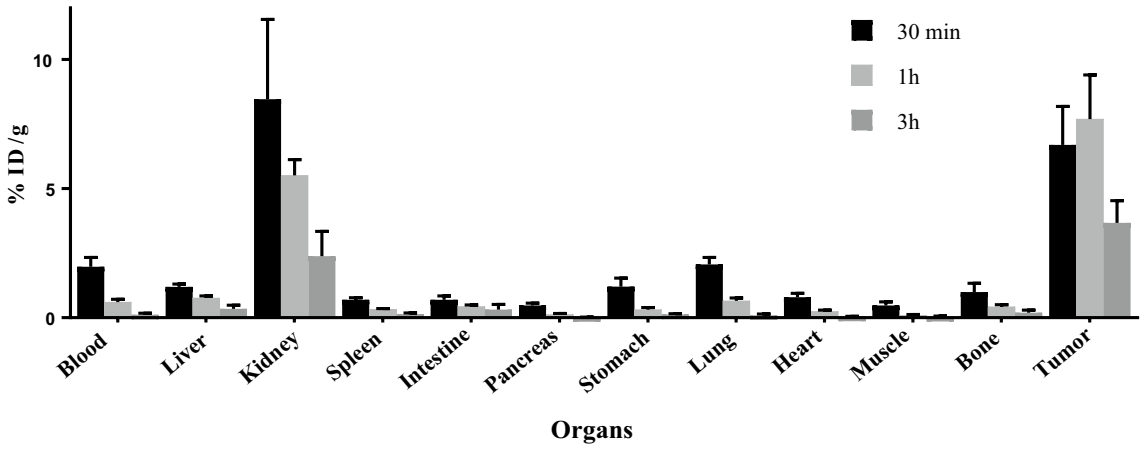

Fig. 4 The biodistribution of $Al^{18}F$-GGNle-$CycMSH_{hex}$ at 30 min, 1 h, and 3 h post-injection in C57BL/6 female mice bearing B16/F10-luc tumors. The data are mean ± standard deviation (%ID/g). Each group's $n \geq 4$

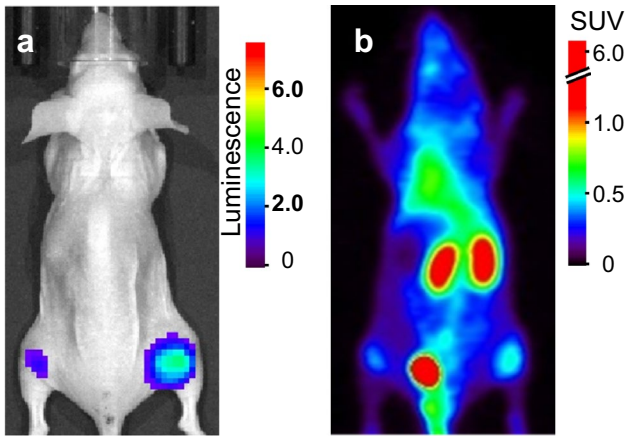

Fig. 5 A representative bioluminescence image (**a**) and PET image of $Al^{18}F$-GGNle-CycMSH$_{hex}$ at 1 h post-injection (**b**) in a nude mouse bearing the B16/F10-luc cell line with different tumor sizes and volumes. Left: 3 mm, 9 mm^3. Right: 4.9 mm, 19.4 mm^3

of traditional ^{18}F-labeling [30, 31]. Since $Al^{18}F$-labeling reaction was almost quantitative, we assume that the use of higher initial radioactivity will enable the production of $Al^{18}F$-NOTA-GGNle-CycMSH$_{hex}$ in specific activity high enough to visualize tumor even in the presence of non-radiolabeled ligand. As observed in our in vitro stability test, the strong bond dissociation energy of Al–F (675 kJ/mol) [32, 33] and the high thermodynamic stability and kinetic inertness of the Al-NOTA complex ensured high in vitro stability of the tracer. Taking these findings collectively along with the high availability of ^{18}F and the simplicity of the radiolabeling process, it is apparent that $Al^{18}F$-NOTA-GGNle-CycMSH$_{hex}$ would be a convenient PET tracer for melanoma.

Our subsequent biological evaluations confirmed that the change of radioisotopes from ^{68}Ga or ^{64}Cu to $Al^{18}F$ does not significantly affect the favorable pharmacokinetics of NOTA-GGNle-CycMSH$_{hex}$ [15, 16, 23]. The rapid blood clearance and high tumor accumulation of $Al^{18}F$-NOTA-GGNle-CycMSH$_{hex}$ resulted in a high tumor-to-blood ratio as early as 30 min post-injection. This result indicates that $Al^{18}F$-NOTA-GGNle-CycMSH$_{hex}$ would provide high contrast in PET imaging even in the early phases. $Al^{18}F$-NOTA-GGNle-CycMSH$_{hex}$ also showed a high tumor-to-background ratio at 3 h post-injection, due to the retained tumor accumulation and the fast whole body clearance.

Although $Al^{18}F$-NOTA-GGNle-CycMSH$_{hex}$ showed high renal accumulation, the excretory pathway for the tracer, high signal in the kidney would not affect the detectability of a primary lesion or major metastatic lesions of melanoma except for adrenal gland metastasis, which commonly metastasize to lung, liver, brain, adrenal gland, gastrointestinal tract, and bone [34, 35]. The low uptake in the bone indicates high in vivo stability of $Al^{18}F$-NOTA-GGNle-CycMSH$_{hex}$ [23]. These results also suggest the potential of $Al^{18}F$-NOTA-GGNle-CycMSH$_{hex}$ as a PET tracer for melanoma detection.

Our PET imaging study revealed high detectability of $Al^{18}F$-NOTA-GGNle-CycMSH$_{hex}$. Considering the physical half-life of ^{18}F (110 min) and the high tumor-to-blood ratio, we performed PET imaging at 1 h post-injection. The use of $Al^{18}F$-NOTA-GGNle-CycMSH$_{hex}$ provided clear images and depicted tumors smaller than 3 mm. Since the tumor thickness is strongly associated with the survival of melanoma patients (94–98% survival for melanomas < 1 mm, 75–88% survival for melanomas 1.01–2 mm, and 24–88% survival for melanomas 2.01–4 mm) [36, 37], early detection plays a significant role for the prognosis.

In addition to the high availability and moderate production cost, the use of ^{18}F has several advantages compared to ^{68}Ga and ^{64}Cu-labeled tracers for the detection of small tumors. For example, the suitable positron energy of ^{18}F (E_{max}: 0.63 MeV) theoretically results in improved spatial resolution compared to that of ^{68}Ga, which has higher positron energy (E_{max}: 1.90 MeV) [38]. The physical half-life of ^{18}F (110 min) may also enable the centralized production and delivery of the tracer to distant satellite centers, whereas the short half-life of ^{68}Ga makes the delivery of sufficient tracer activities to remote centers challenging. In contrast, ^{64}Cu has positron energy (E_{max}: 0.66 MeV) that is comparable to that of ^{18}F, but the physical half-life of ^{64}Cu (12.7 h) is too long for peptide-based tracers with rapid pharmacokinetics, which may cause unnecessary radiation exposure to the patients. Although one-by-one comparisons are necessary, $Al^{18}F$-NOTA-GGNle-CycMSH$_{hex}$ may overcome the limitations related to the uses of ^{68}Ga and ^{64}Cu and would thus warrant further clinical investigation.

In conclusion, we successfully prepared $Al^{18}F$-NOTA-GGNle-CycMSH$_{hex}$ with a high radiochemical yield. $Al^{18}F$-NOTA-GGNle-CycMSH$_{hex}$ showed high tumor accumulation and rapid clearance from non-target organs in melanoma-bearing mice. The use of $Al^{18}F$-NOTA-GGNle-CycMSH$_{hex}$ enabled the clear visualization of very small tumors in PET imaging. These findings suggest that $Al^{18}F$-NOTA-GGNle-CycMSH$_{hex}$ would be a promising PET tracer for melanoma imaging at early stages.

References

1. Apalla Z, Lallas A, Sotiriou E, Lazaridou E, Ioannides D. Epidemiological trends in skin cancer. Dermatol Pract Concept. 2017;7:1–6.
2. Huff LS, Chang CA, Thomas JF, Cook-Shimanek MK, Blomquist P, Konnikov N, et al. Defining an acceptable period of time from melanoma biopsy to excision. Dermatol Rep. 2012;4:e2.

3. Danielsen M, Højgaard L, Kjær A, Fischer BM. Positron emission tomography in the follow-up of cutaneous malignant melanoma patients: a systematic review. Am J Nucl Med Mol Imaging. 2013;4:17–28.
4. Xing Y, Bronstein Y, Ross MI, Askew RL, Lee JE, Gershenwald JE, et al. Contemporary diagnostic imaging modalities for the staging and surveillance of melanoma patients: a meta-analysis. J Natl Cancer Inst. 2011;103:129–42.
5. Pilat P, Borzecki A, Jazienicki M, Krasowska D. Skin melanoma imaging using ultrasonography: a literature review. Postep Dermatol Alergol. 2018;35:238–42.
6. Crippa F, Leutner M, Belli F, Gallino F, Greco M, Pilotti S, et al. Which kinds of lymph node metastases can FDG PET detect? A clinical study in melanoma. J Nucl Med. 2000;41:1491–4.
7. Mijnhout GS, Hoekstra OS, van Tulder MW, Teule GJ, Devillé WL. Systematic review of the diagnostic accuracy of ^{18}F-fluorodeoxyglucose positron emission tomography in melanoma patients. Cancer. 2001;91:1530–42.
8. Tchernev G, Popova LV. PET scan misses cutaneous melanoma metastasis with significant tumour size and tumour thickness. Open Access Maced J Med Sci. 2017;5:963–6.
9. Uğurluer G, Kibar M, Yavuz S, Kuzucu A, Serin M. False positive ^{18}F-FDG uptake in mediastinal lymph nodes detected with positron emission tomography in breast cancer: a case report. Case Rep Med. 2013;2013:459753.
10. Dimitrakopoulou-Strauss A, Strauss LG, Burger C. Quantitative PET studies in pretreated melanoma patients: a comparison of 6-[^{18}F]fluoro-L-dopa with ^{18}F-FDG and ^{15}O-water using compartment and noncompartment analysis. J Nucl Med. 2001;42:248–56.
11. Guo H, Shenoy N, Gershman BM, Yang J, Sklar LA, Miao Y. Metastatic melanoma imaging with an ^{111}In-labeled lactam bridge-cyclized α-melanocyte-stimulating hormone peptide. Nucl Med Biol. 2009;36:267–76.
12. Quinn T, Zhang X, Miao Y. Targeted melanoma imaging and therapy with radiolabeled alpha-melanocyte stimulating hormone peptide analogues. G Ital Dermatol Venereol. 2011;145:245–58.
13. Miao Y, Benwell K, Quinn TP. ^{99m}Tc- and ^{111}In-labeled alpha-melanocyte-stimulating hormone peptides as imaging probes for primary and pulmonary metastatic melanoma detection. J Nucl Med. 2007;48:73–81.
14. Siegrist W, Solca F, Stutz S, Giuffrè L, Carrel S, Girard J, et al. Characterization of receptors for α-melanocyte-stimulating hormone on human melanoma cells. Cancer Res. 1989;49:6352–8.
15. Guo H, Miao Y. Cu-64-labeled lactam bridge-cyclized α-MSH peptides for PET imaging of melanoma. Mol Pharm. 2012;9:2322–30.
16. Guo H, Gallazzi F, Miao Y. Gallium-67-labeled lactam bridge-cyclized alpha-MSH peptides with enhanced melanoma uptake and reduced renal uptake. Bioconjug Chem. 2012;23:1341–8.
17. Orbay H, Zhang Y, Valdovinos HF, Song G, Hernandez R, Theuer CP, et al. Positron emission tomography imaging of CD105 expression in a rat myocardial infarction model with ^{64}Cu-NOTA-TRC105. Am J Nucl Med Mol Imaging. 2013;4:1–9.
18. Decristoforo C, Pickett RD, Verbruggen A. Feasibility and availability of ^{68}Ga-labelled peptides. Eur J Nucl Med Mol Imaging. 2012;39:S31–40.
19. Pfeifer A, Knigge U, Binderup T, Mortensen J, Oturai P, Loft A, et al. ^{64}Cu-DOTATATE PET for neuroendocrine tumors: a prospective head-to-head comparison with ^{111}In-DTPA-Octreotide in 112 patients. J Nucl Med. 2015;56:847–54.
20. Zhang C, Zhang Z, Lin KS, Lau J, Zeisler J, Colpo N, et al. Melanoma imaging using ^{18}F-Labeled α-melanocyte-stimulating hormone derivatives with positron emission tomography. Mol Pharm. 2018;15:2116–22.
21. Cai H, Conti PS. RGD-based PET tracers for imaging receptor integrin αvβ3 expression. J Label Compd Radiopharm. 2013;56:264–79.
22. Preshlock S, Tredwell M, Gouverneur V. ^{18}F-labeling of arenes and heteroarenes for applications in positron emission tomography. Chem Rev. 2016;116:719–66.
23. Lang L, Li W, Guo N, Ma Y, Zhu L, Kiesewetter DO, et al. Comparison study of [^{18}F]FAl-NOTA-PRGD2, [^{18}F] FPPRGD2, and [^{68}Ga]Ga-NOTA-PRGD2 for PET imaging of U87MG tumors in mice. Bioconjug Chem. 2011;22:2415–22.
24. McBride WJ, D'Souza CA, Sharkey RM, Karacay H, Rossi EA, Chang CH, et al. Improved ^{18}F labeling of peptides with a fluoride-aluminum-chelate complex. Bioconjug Chem. 2010;21:1331–40.
25. Wan W, Guo N, Pan D, Yu C, Weng Y, Luo S, et al. First experience of ^{18}F-alfatide in lung cancer patients using a new lyophilized kit for rapid radiofluorination. J Nucl Med. 2013;54:691–8.
26. Liu T, Liu C, Xu X, Liu F, Guo X, Li N, et al. Preclinical evaluation and pilot clinical study of Al^{18}F-PSMA-BCH for prostate cancer imaging. J Nucl Med. 2019. https://doi.org/10.2967/jnumed.118.221671.
27. Shamshirian D, Erfani M, Beiki D, Fallahi B, Shafiei M. Development of a ^{99m}Tc-labeled lactam bridge-cyclized alpha-MSH derivative peptide as a possible single photon imaging agent for melanoma tumors. Ann Nucl Med. 2015;29:709–20.
28. Richter S, Wuest F. ^{18}F-labeled peptides: the future is bright. Molecules. 2014;19:20536–56.
29. Bhattacharyya S, Dixit M. Metallic radionuclides in the development of diagnostic and therapeutic radiopharmaceuticals. Dalton Trans. 2011;40:6112–8.
30. Shively JE. ^{18}F labeling for immuno-PET: where speed and contrast meet. J Nucl Med. 2007;48:170–2.
31. Jacobson O, Kiesewetter DO, Chen X. Fluorine-18 radiochemistry, labeling strategies and synthetic routes. Bioconjug Chem. 2015;26:1–18.
32. McBride WJ, Sharkey RM, Karacay H, D'Souza CA, Rossi EA, Laverman P, et al. A novel method of ^{18}F radiolabeling for PET. J Nucl Med. 2009;50:991–8.
33. Farkas E, Fodor T, Kálmán FK, Tircsó G, Tóth I. Equilibrium and dissociation kinetics of the [Al(NOTA)] complex (NOTA = 1,4,7-triazacyclononane-1,4,7-triacetate). React Kinet Mech Catal. 2015;116:19–33.
34. Tas F. Metastatic behavior in melanoma: timing, pattern, survival, and influencing factors. J Oncol. 2012;2012:647684.
35. Patel JK, Didolkar MS, Pickren JW, Moore RH. Metastatic pattern of malignant melanoma. A study of 216 autopsy cases. Am J Surg. 1978;135:807–10.
36. Tejera-Vaquerizo A, Nagore E, Meléndez JJ, López-Navarro N, Martorell-Calatayud A, Herrera-Acosta E, et al. Chronology of metastasis in cutaneous melanoma: growth rate model. J Invest Dermatol. 2012;132:1215–21.
37. Gershenwald JE, Scolyer RA. Melanoma staging: American Joint Committee on Cancer (AJCC) 8th edition and beyond. Ann Surg Oncol. 2018;25:2105–10.
38. Lodge MA, Leal JP, Rahmim A, Sunderland JJ, Frey EC. Measuring PET spatial resolution using a cylinder phantom positioned at an oblique sngle. J Nucl Med. 2018;59:1768–75.